

# Arm Trajectory Planning by Controlling the Direction of End-point Position Error Caused by Disturbance

Tasuku YAMAWAKI and Masahito YASHIMA

Dept. of Mechanical Systems Engineering

National Defense Academy of Japan

Yokosuka, Kanagawa 239-8686, JAPAN

{yamawaki, yashima}@nda.ac.jp

**Abstract**—The present paper proposes the control algorithm of direction of the end-point position error caused by the disturbance. Taking consideration of it, the effect of the disturbance on the end-point position is maximized in the direction of the singular vector corresponding to the maximum singular value. Therefore, if we can control the direction of the singular vector, we will be able to control the direction of the positional error of the end-point position steered by the disturbance. We propose the control algorithm of the direction of the positional error and the effectiveness by applying the algorithm to the hitting motion by the robotic arm.

## I. INTRODUCTION

In general, we cannot obtain nominal models of real robotic systems, because the real robotic systems include various uncertainty. One of the uncertainty is noise and disturbance which are excluded from the nominal models. For example, sensor noise and quantization error of the angular velocity are applied to the robot as disturbance. To constrain the disturbance, many researchers focus on the controller design such as the robust control [2], [7]. The controller design is very complicated.

In the meanwhile, our concept is effectively making use of the robot dynamics to accomplish the task robustly even though the controller is very simple. Therefore we focus on the motion planning rather than the controller design. If we can obtain the robust trajectory independently of the control input, the controller can be simplified. Our approach is to plan the motion which reduces the influence of the disturbance on the task by utilizing the robot dynamics aggressively. To our knowledge, while the motion planings for robotic arms have been proposed [1], [9], [8], none of these schemes have been addressed to constrain the disturbance.

We have revealed that our approach is effective to reduce the magnitude of the end-point positional error at the final point of the trajectory [10]. On the other hand, the present paper focuses on the generation direction of the end-point positional error. In several tasks, the generation direction of the positional error is more important than the magnitude of it. One of such task is the hitting motion by the robotic arm as shown in Fig. 1. If the end-point is deviated vertically to the desired trajectory by disturbance, the robot fails to hit the target as described in Fig. 1(a). If the direction of the positional error can be controlled to be tangential to the desired trajectory as shown in Fig. 1(b), the robotic arm can hit the target even though the disturbance is applied. For

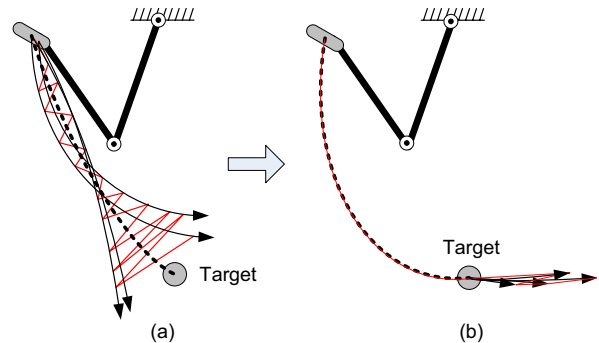


Fig. 1. Application examples of the control of direction of the end-point position error caused by disturbance

the hitting motion, there is no need to force the robotic arm to reduce the magnitude of the positional error. If only the generation direction of the positional error can be controlled, we will be able to improve the robustness of the hitting motion to the disturbance. Therefore the present paper deals with only the generation direction of the end-point positional error and proposes the technique to control the generation direction to the tangential direction of the target path.

The robotic arm can be regarded as the control system of which the input and the output are the joint torque and the end-point position, respectively. From the linear system theory, the magnitudes of the singular values of the output controllability matrix represent the strengths of the effects of input on output [3], [4]. Therefore, the singular vector corresponding to the maximum singular value indicates the direction in which the effect of the joint torque (input) on the position (output) of the end-effector is maximized. This implies that the singular vector also indicate the direction in which the effect of the disturbance have the maximum intensity with the end-point position. Thus if we can plan the robot motion to control appropriately the direction of the singular vector, we will be able to plan the generation direction of the end-point positional error caused by the disturbance.

The direction of the singular vector is determined from only the robot dynamics and thus independent from the control input. Therefore we can control the generation direction of the end-point positional error with the simple controller.

To verify the validity of our approach, we conduct two



and output variables, respectively. The inertia matrix  $M$  and the centrifugal force vector  $h$  are given as

$$M = \begin{bmatrix} 1.151 + 0.0828 \cos \theta_2 & 0.0758 + 0.0414 \cos \theta_2 \\ 0.0758 + 0.0414 \cos \theta_2 & 0.0758 \end{bmatrix} \quad (11)$$

$$h = \begin{bmatrix} -0.0828 \dot{\theta}_1 \dot{\theta}_2 \sin \theta_2 - 0.0414 \dot{\theta}_2^2 \sin \theta_2 \\ 0.0414 \dot{\theta}_1^2 \sin \theta_2 \end{bmatrix} \quad (12)$$

which are obtained by the identification experiment of the direct-drive robotic arm applied to the experiment described later.

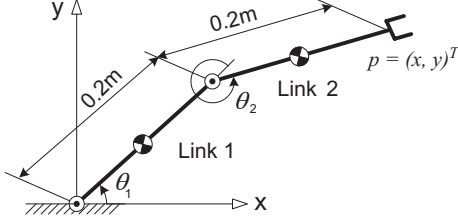


Fig. 2. Two joint robotic arm which moves within a horizontal plane.

The joint torque to trace the nominal end-point's trajectory is obtained using the equation of motion (1) and the kinematic equation (2) in advance. The input torque is set as the sum of its nominal joint torque and the Gaussian white noise. Applying the input torque to the feedforward controller, we obtain the locus of the end-point. This simulation is repeated 50 times and obtain the variance of the end-point position error caused by the disturbance.

We set the nominal trajectory of the end-point as the straight line connecting the start to the goal. Assuming that the velocity and acceleration of the end-point at both ends are zero, we can obtain the nominal trajectory as

$$p(t) = p_0 + (15t_n^4 - 6t_n^5 - 10t_n^3) (p_0 - p_f), \quad (13)$$

where  $t_n$  is normalized time given by dividing elapsed time  $t$  by the total motion time  $t_f$ , which can be described as  $t_n = t/t_f$ .

We let the start and goal be  $p_0 = (0.22, 0)^T$  m and  $p_f = (0.31, 0.225)^T$  m, the total motion time  $t_f$  be 0.4 sec, and the variance of the Gaussian white noise be  $(9, 9)$  N<sup>2</sup>m<sup>2</sup>. Fig. 3 shows nominal arm movement and the singular vectors at each end-point position at  $t = 0, 0.08, 0.16, 0.24, 0.32, 0.40$  sec. Fig. 4 shows the position error distribution denoted by  $\times$ . The center position of each figure indicates the nominal position of the end-point at each time step. The straight line indicates the direction of the singular vector at each nominal end-point position.

According to the simulation results, the end-point deviates from nominal end-point position by the disturbance. However, the end-point constantly converges near onto the singular vector, even though the direction of the singular vector changes with the arm movement.

If we can fit the direction of the singular vector to the tangential direction of the nominal trajectory, we will be

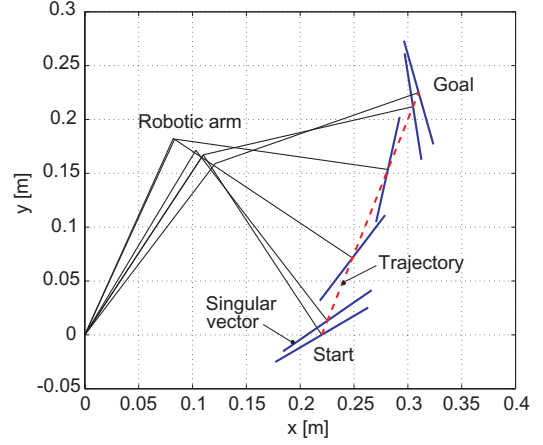


Fig. 3. Singular vectors at each end-point position in a straight line trajectory

able to obtain the robust trajectory from which the end-point suffered from the disturbance never deviate greatly. The following section describes the motion planning which enables the singular vector to point toward the tangential direction of the trajectory as much as possible.

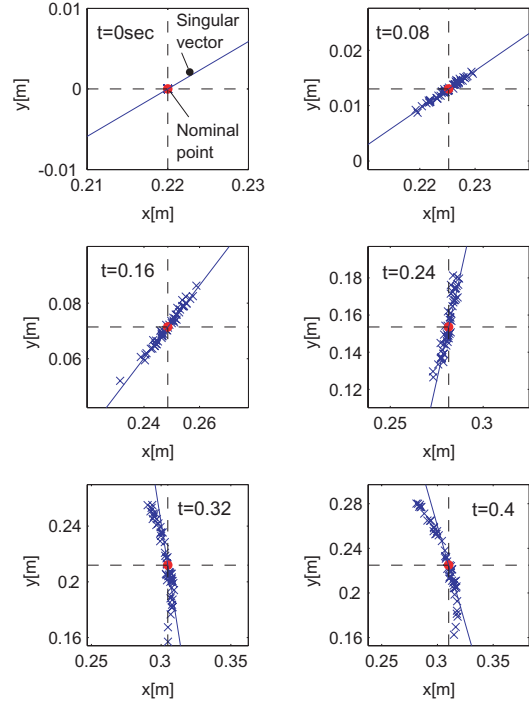


Fig. 4. Position error distribution and singular vector at each nominal end-point position.

#### IV. MOTION PLANNING IN CONSIDERATION OF GENERATION DIRECTION OF END-POINT POSITION ERROR

This section discusses the motion planning which fits the direction of the singular vector to the tangential direction of the trajectory as much as possible. In Fig. 5, the thin lines drawn in the  $xy$ -plane are the singular vector at each

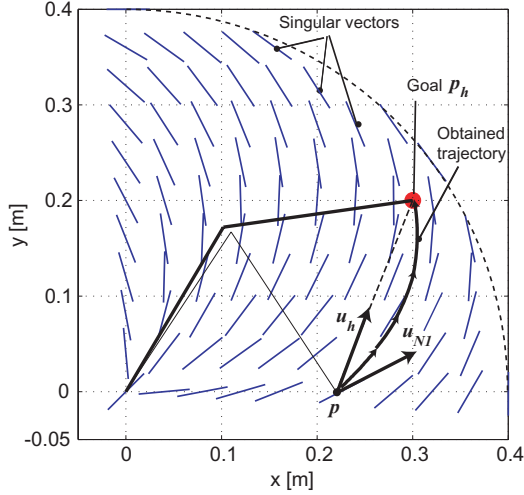


Fig. 5. Singular vectors and the trajectory obtained by the proposed motion planning

end-point position and the thick curve represents the end-point's trajectory obtained by the motion planning proposed in this section. The end-point moving along the singular vector reaches the goal  $p_h$  finally.

The trajectory generation algorithm is based on the concept of the potential functions [5]. We make the virtual force  $f_p \in \mathbb{R}^m$  act on the end-point, which are given as the sum of three virtual forces as follows:

$$f_p = f_s + f_h + f_d \quad (14)$$

The first one is  $f_s \in \mathbb{R}^m$  acting toward the direction of the singular vector. The second one is the attractive force to the goal  $f_h \in \mathbb{R}^m$ . The third one is the damping force  $f_d \in \mathbb{R}^m$ . Each force is given by

$$f_s = k_s \|\mathbf{p}_h - \mathbf{p}\| \operatorname{sgn}\{\mathbf{u}_{N1}^T(\mathbf{p}_h - \mathbf{p})\} \mathbf{u}_{N1} \quad (15)$$

$$f_h = k_h \mathbf{u}_h \quad (16)$$

$$f_d = -k_d \dot{\mathbf{p}}, \quad (17)$$

where  $k_s$ ,  $k_h$  and  $k_d$  are gains. As shown in Fig. 5,  $\mathbf{u}_h$  is the unit vector indicating to the goal  $p_h$  from the current end-point  $p$ , and  $\mathbf{u}_{N1}$  is the singular vector obtained from (9), whose direction is determined by the  $\operatorname{sgn}$  function. We let the magnitude of the attracting force  $f_h$  constant to gain the enough velocity at the goal.

From equations (14) to (17), the relative magnitude of the three virtual forces  $f_h$ ,  $f_s$  and  $f_d$  are defined by the relative value of the three gains  $k_s$ ,  $k_h$  and  $k_d$ . Thus, there are a number of design choices to get the nominal trajectory. Here, the influence given by the three gains is described.

The gain  $k_s$  controls the relative influence of the virtual force acting toward the direction of the singular vector. If we choose to weight its value more heavily than the others, we will obtain the trajectory which enables the singular vector to point toward the tangential direction of the trajectory. However, the relative influence of the attractive force becomes small. The obtained trajectory may need a long time for the end-point to reach the goal.

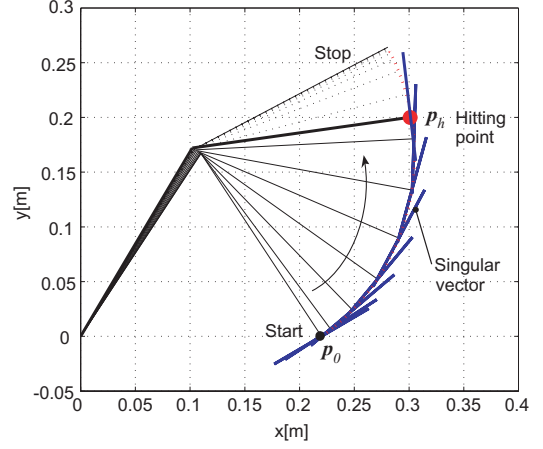


Fig. 6. Nominal trajectory obtained by the proposed trajectory generator

The gain  $k_h$  controls the relative influence of the attractive force. If we choose to weight its value more heavily than the others, we will obtain the trajectory, in which the end-point is quickly attracted to the goal. However, the relative influence of the virtual force acting toward the direction of the singular vector becomes small. Thus the singular vector of the obtained trajectory does not point toward the tangential direction of the trajectory.

The gain  $k_d$  controls the relative influence of the damping force. If we choose to weight its value more heavily than the others, the movement of the end-point will be slow. If we set the other gains as zero, the magnitude of the braking force can be controlled.

Finally, the joint torque  $\tau(t)$  at time  $t$  can be given by

$$\tau(t) = \mathbf{J}^T(t) f_p(t) \quad (18)$$

The joint angle  $\theta(t + \Delta t)$  at time  $t + \Delta t$  is obtained by the numerical integration of  $\dot{\theta}(t)$  given by substituting  $\tau(t)$  for the motion equation (1).

## V. APPLICATION TO HITTING MOTION

This section numerically and experimentally verifies that, by applying the proposed motion planning, the robotic arm can hit the target robustly.

### A. Trajectory Planning

We apply the proposed algorithm to the two-DOF robotic arm shown in Fig. 2 and obtain the nominal trajectory. Let the start point  $p_0 = (0.22, 0)^T$  m, the hitting point  $p_h = (0.3, 0.2)^T$  m. The gains are set as described in Table I, where  $t_h$  is the hitting time when the end-point reaches  $\|\mathbf{p}_h - \mathbf{p}\| < D_t/2$ , assuming that the target is round shape with a diameter,  $D_t = 10$  mm. While  $t > t_h$ , to stop the motion, we affect only  $f_d$  as the braking force. If the end-point velocity satisfies  $\|\dot{\mathbf{p}}\| < 0.005$  m/s, we stop generating the trajectory.

Figure 6 shows the trajectory obtained by the proposed algorithm and the singular vectors at each end-point position. The obtained trajectory is curved and passes fairly close to

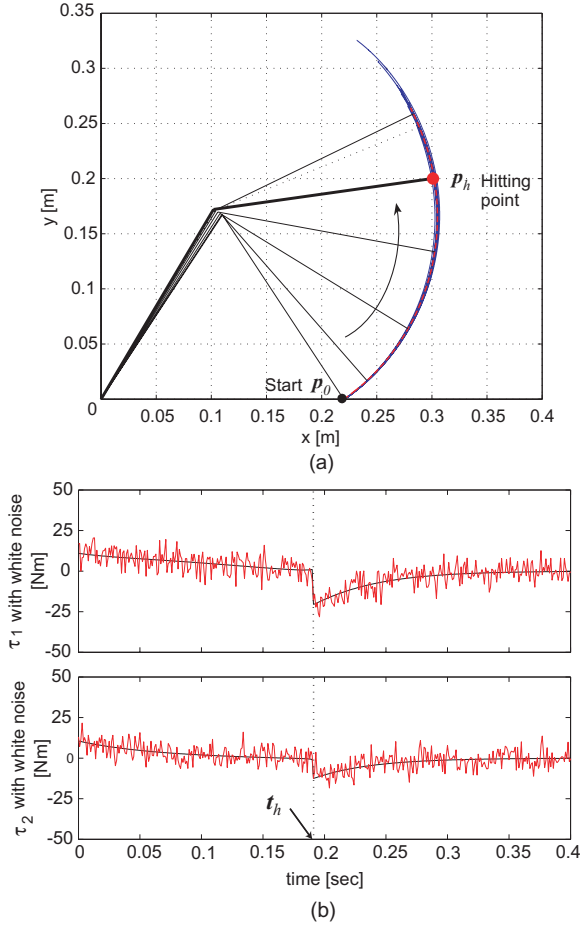


Fig. 7. Simulation results for feed-forward controller based on the proposed trajectory generation algorithm. (a) arm movement distributions and (b) input torque profiles.

the hitting point. The singular vectors obviously point toward the tangential direction of the trajectory. This yields that the proposed algorithm enables the singular vector to point toward the tangential direction of the trajectory.

### B. Position Error Caused by Disturbance

The simulation results in section III-B make it obvious that the position error of the end-point converges onto near the singular vector. In this section, we obtain the end-point locus of the robotic arm controlled by the joint torque including the disturbance. The nominal joint torque is obtained from the proposed trajectory generation algorithm in advance. The input torque is set as the sum of its nominal joint torque and the Gaussian white noise. Applying the input torque to the

TABLE I  
VALUES OF GAIN PARAMETERS FOR THE MOTION PLANNING

State	$k_s$	$k_h$	$k_d$
$t \leq t_h$ (Before hitting)	35	75	30
$t > t_h$ (After hitting)	0	0	40

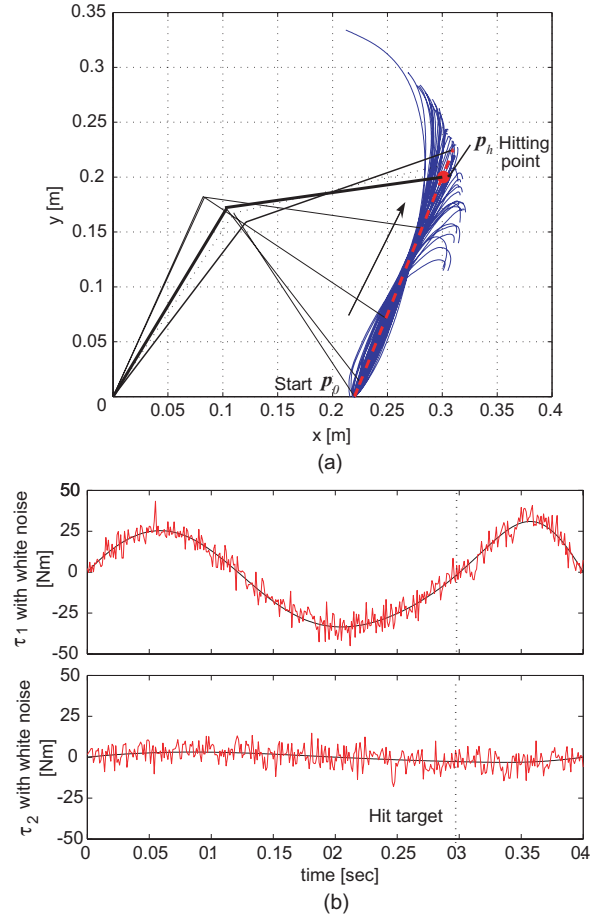


Fig. 8. Simulation results for feed-forward controller based on the straight line trajectory. (a) arm movement distributions and (b) input torque profiles.

feedforward controller, we obtain the locus of the end-point. For comparison, we also apply a feedforward controller to the straight line trajectory obtained in section III-B. These two simulations are repeated 50 times. The variance of the Gaussian white noise is set as  $(25, 25) \text{ N}^2\text{m}^2$ .

Figure 7 (a) describes the loci of the end-point obtained by controlling the direction of the singular vector to be tangential to the trajectory utilizing the propose algorithm. Fig. 7 (b) shows its input torque, where, at hitting time  $t = t_h$ , the input torques discontinuously change because the value of the gains are changed as shown in Table I. Fig. 8 (a) and (b) describe the simulation result of the straight line trajectory. The loci of Fig. 7 converges closer to the nominal trajectory than that of Fig. 8. According to these results, by controlling the direction of the singular vector to be tangential to the trajectory, we can implement the robust motion which can keep the end-point of the robotic arm close to the nominal trajectory, even if the input torque includes the disturbance.

### C. Experiment

This section verifies experimentally that the trajectory obtained by the proposed algorithm is robust to the disturbance.

We apply the obtained trajectory to the two-DOF robotic arm. Figure 9 shows the two-DOF direct-drive arm (SR-402DD(s), Tokyo Electronic Systems Corp.) whose physical parameters are obtained by the identification experiment, which are described in (11) and (12). The assuming task is hitting the ball, of which diameter is  $D_t = 10\text{mm}$ , by the cylindrical bat installed at the end-point of the robotic arm, of which diameter is  $D_b = 6\text{mm}$ . We let the start point and the hitting point be same as Fig. 7. Thus the trajectory obtained in section V-A can be applied to this task. The input torque is set as the sum of its nominal joint torque and the Gaussian white noise. Applying the input torque to the feedforward controller, we obtain the locus of the end-point. For comparison, we also apply a feedforward controller to the straight line trajectory obtained in section III-B. The hitting task is repeated 50 times. The variance of the Gaussian white noise is set as  $(25, 25) \text{ N}^2\text{m}^2$ .

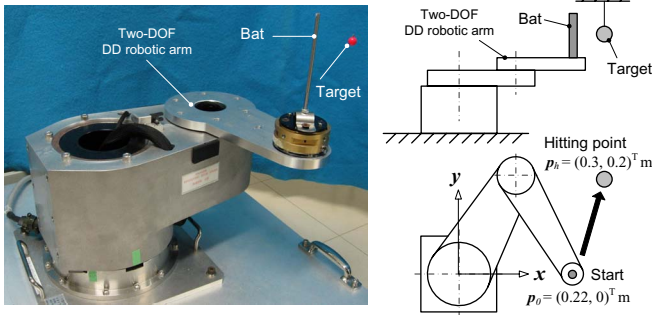


Fig. 9. Experimental set-up

Figure 10 describes the loci of the end-point obtained by controlling the direction of the singular vector to be tangential to the trajectory utilizing the propose algorithm. Fig. 11 describe the experimental result of the straight line trajectory. The loci of Fig. 10 converges closer to the nominal trajectory than that of Fig. 11. While the robotic arm applied the straight line trajectory hits the target 18 out of 50 times (its batting average is 36%), the robotic arm applied the proposed algorithm achieves to hit the target 50 out of 50 times (its batting average is 100%). According to these experimental results, by controlling the direction of the singular vector to be tangential to the trajectory, we can implement the robust motion which can keep the end-point of the robotic arm close to the nominal trajectory, even if the input torque includes the disturbance.

This section experimentally reveals that the control of direction of the singular vector is very effective approach for robotic arms to achieve high robustness.

## VI. CONCLUSION

The present paper revealed that (1) the positional error of the end-point converged onto near the singular vector of the output controllability matrix, (2) the proposed trajectory generation algorithm enabled the singular vector to point toward the tangential direction of the trajectory, and (3) the end-point of the robotic arm could be controlled close to the nominal trajectory by using the proposed trajectory

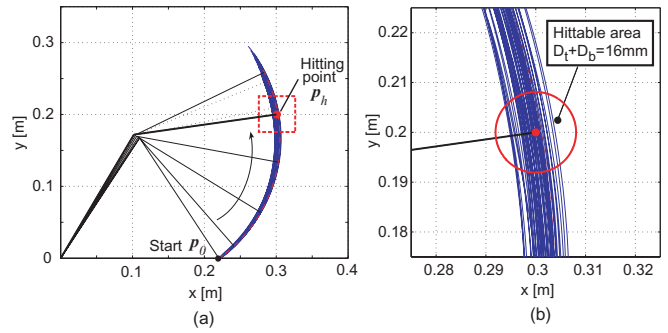


Fig. 10. Experimental results for feed-forward controller based on the proposed trajectory generation algorithm. (a) arm movement distributions and (b) extended figure around the hitting point.

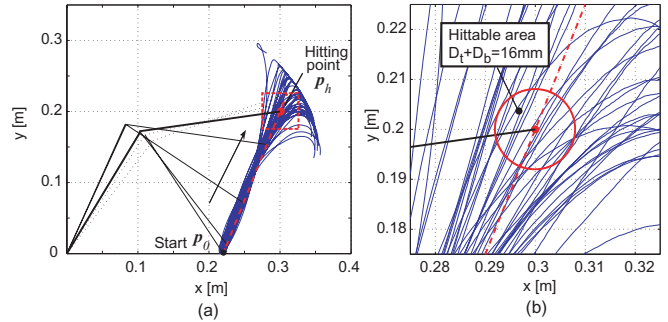


Fig. 11. Experimental results for feed-forward controller based on the straight line trajectory. (a) arm movement distributions and (b) extended figure around the hitting point.

planning algorithm, even though the input torque includes the disturbance. Our future work is to propose the new trajectory generation algorithm including the orientation error.

## REFERENCES

- [1] J.E. Bobrow, S. Dubowsky, and J.S. Gibson, "Time-optimal Control of Robotic Manipulators Along Specified Paths," *Int. J. Robotics Research*, vol.4, no. 3, pp. 3-17, 1985.
- [2] J.C. Doyle, K. Glover, P.P. Khargonekar, and B.A. Francis, "State-Space Solutions to Standard  $\mathcal{H}_2$  and  $\mathcal{H}_\infty$  control problem," *IEEE Trans. Automatic Control*, vol. 34, no. 8, pp. 831-847, 1989.
- [3] B. Friedland, "Controllability Index based on Conditioning Number," *Trans. of ASME, J. Dynamics Systems, Measurement and Control*, pp. 444-445, December 1975.
- [4] C.D. Johnson, "Optimization of a Certain Quality of Complete Controllability and Observability for Linear Dynamical Systems," *Trans. of ASME, J. Basic Engineering*, pp.228-238, June 1969.
- [5] O. Khatib, "Real-Time Obstacle Avoidance for Manipulators and Mobile Robots," *Int. J. Robotics Research*, vol.5, no. 1, pp. 90-98, 1986.
- [6] E. Kreindler and P.E. Sarachik, "On the Concepts of Controllability and Observability of Linear Systems," *IEEE Trans. on Automatic Control*, vol. 9, no. 2, pp. 129-136, 1964.
- [7] J. Paattilammi and P.M. Mäkilä, "Fragility and Robustness: A case study on Paper Machine Headbox Control," *IEEE Control System Magazine*, vol. 20, no. 1, pp.13-22, 2000.
- [8] E. Plaky and L.E. Kavraki, "Distributed Sampling-based Roadmap of Trees for Large-scale Motion Planning," *Proc. of the 2005 IEEE International Conference on Robotics and Automation*, pp. 3879-3884, 2005.
- [9] Z. Shiller and S. Dubowsky, "On Computing the Global Time-optimal Motions of Robotic Manipulators in the Presence of Obstacle," *IEEE Trans. on Robotics and Automation*, vol. 7, no. 6, pp. 785-797, 1991.
- [10] T. Yamawaki and M. Yashima, "Effect of Gravity on Manipulation Performance of a Robotic Arm," *Proc. of the 2007 IEEE International Conference on Robotics and Automation*, pp. 4407-4413, 2007.